Analysis, Modeling, and Measurement of Shielding Effectiveness for a Cylindrical Waveguide with a Hexagonal Insert Structure

Scott W. Faust [1] and Daniel N. Aloi [2]

[1] Vehicle Electronics and Architecture
U.S. Army TARDEC, Warren, Michigan 48397-5000, United States of America
scott.w.faust.civ@mail.mil

[2] Department of Electrical and Computer Engineering
Oakland University, Rochester, Michigan 48309-4479, United States of America
aloi@oakland.edu

Abstract – A theoretical model is presented for the shielding effectiveness of a waveguide containing an insert consisting of several smaller hexagonal or "honeycomb"-shaped waveguides. FEKO, an electromagnetic modeling software package, is used to create computer-aided design (CAD) models of physical waveguides, and to find solutions for the TE_{11} mode of propagation for each model using the Finite Element Method (FEM). S-parameters are used to characterize the shielding effectiveness of the waveguide models through simulation in FEKO and measurement of waveguide samples in the laboratory. The results obtained by each method are compared and discussed.

Index Terms – Attenuation, computer-aided design, cutoff frequency, electromagnetic compatibility, finite element method, honeycomb insert, shielding effectiveness, S-parameters, simulation, waveguides.

I. INTRODUCTION

Preparation for electromagnetic compatibility (EMC) testing of liquid-cooled power electronics requires selection of waveguides to pass the coolants in and out of the shielded enclosure. Various waveguide manufacturers provide basic calculations for the cutoff frequency of a circular waveguide pipe penetration based on the diameter and length of the waveguide. Optional "honeycomb" inserts are then quoted as an option to increase the cutoff frequency when the waveguide is loaded with materials other than air, i.e., fluids for cooling, fire suppression, etc. with limited information provided on the efficacy of the honeycomb insert. The attenuation of the overall honeycomb insert structure is typically stated to be that of a single waveguide in the insert. This information is typically limited to the cutoff frequency of the individual insert, leaving the end user unable to determine the crossover point where the shielding effectiveness of the waveguide is less than the

rated shielding effectiveness of the enclosure in which it is installed. McInerney et al. (1984) provided limited data on the shielding effectiveness of waveguides filled with various fluids over a limited frequency range (up to 7.5 GHz), including the predicted shielding effectiveness for a waveguide having an insert containing circular apertures. The shielding effectiveness of this insert was attributed to a single aperture within the insert structure [1]. Other authors review waveguides and their use in maintaining shielding effectiveness, with no analytic formula provided to estimate the shielding effectiveness of the waveguide based on the dimensions or number of openings in the honeycomb insert [2, 3, 4].

The goals of this paper are to present a theoretical model for the shielding effectiveness of a waveguide with a honeycomb insert having *N* individual inserts, develop a suitable model for simulation using electromagnetic modeling software, and compare the results obtained through analysis and modeling with measurements of commercially-available waveguides up to 34 GHz.

II. THEORETICAL MODEL

Prior work developed and proposed three theoretical models for a cylindrical waveguide having a honeycomb insert [5]. Each model used a first-order approximation of a single hexagonal "honeycomb" insert as a circular waveguide. This approximation is illustrated by Fig. 1.
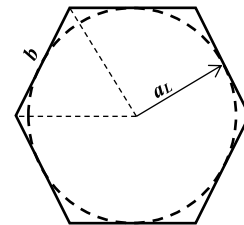
Fig. 1. Circle approximation for the cross-section of a single hexagonal "honeycomb" waveguide insert [5].

This approximation of the hexagonal insert as a circular waveguide simplifies the calculation of the estimated cutoff frequency for the insert by using the well-known equation for the cutoff frequency of a circular waveguide for the dominant mode of propagation, TE_{11} [6]:

$$f_c = \frac{\chi'_{11}}{2\pi a \sqrt{\mu \varepsilon}}, \qquad (1)$$

where $\chi'_{11} = 1.8412$ is the zero of the derivative of the Bessel function for TE_{11}, a is the radius of the circle inscribed within the hexagonal cross-section in meters, μ the permeability, and ε the permittivity of the material within the insert.

The attenuation, or shielding effectiveness of a circular waveguide for a particular mode is:

$$A = 54.58 f L \left[\mu \varepsilon \left(\left(\frac{f_c}{f} \right)^2 - 1 \right) \right]^{\frac{1}{2}}, \qquad (2)$$

where A is the attenuation of the waveguide in decibels, f is the frequency of the electromagnetic wave propagating through the waveguide, L is the length of the waveguide, and f_c the cutoff frequency of the waveguide [2-5]. In writing analytic expressions for the cutoff frequency of a waveguide with a honeycomb insert, the cutoff frequency of the main waveguide, i.e., the waveguide containing the honeycomb insert, is denoted by f_c, whereas the cutoff frequency of an individual insert within the honeycomb structure is represented by $f_{c,insert}$.

Of the three analytic models proposed, preliminary modeling and simulation efforts using FEKO identified one particular model as having the lowest average error between the theoretical and simulation results as compared to other proposed models [5]. This particular model was based on a proposal by Kaiser (2006), that shielding effectiveness of a single opening is improved by dividing its cross-sectional area into N smaller openings [7]. The resulting formula for the shielding effectiveness of the honeycomb insert using this model is [5]:

$$SE \cong 54.58 f L_{insert} \left[\mu \varepsilon \left(\left(\frac{f_{c,insert}}{f} \right)^2 - 1 \right) \right]^{\frac{1}{2}}$$
$$+ 10 \log_{10} N, \qquad (3)$$

where L_{insert} is the length of an individual insert.

Equation (3) calculates the shielding effectiveness of a circular waveguide having a honeycomb insert as the shielding effectiveness of a single insert and an attenuation factor based on N smaller inserts or waveguides, with one condition placed on the diameter of a single insert:

$$2a_L < \frac{\lambda}{10}. \qquad (4)$$

This condition requires that the diameter of an individual insert be electrically small when compared to the wavelength of the electromagnetic wave incident upon the insert [8].

Two formulas are available to calculate $f_{c,insert}$ for the TE_{11} mode of propagation for the hexagonal insert. The first formula relies on the approximation of the hexagonal as shown in Fig. 1, and the application of equation (1). A second formula, not utilized in the prior work [5], was proposed by Ravelo and Mazari (2010). It applies to a waveguide whose cross-sectional area may be represented as an nth-order polygon. This formula may be written as:

$$f_{c,insert}(n) = \frac{\chi'_{11}}{4\pi b \sqrt{\mu \epsilon}} \left[1 + \sec \left(\frac{\pi}{n} \right) \right], \qquad (5)$$

with $n=6$ for a hexagonal insert [9]. Both equations (1) and (5) were used as part of MATLAB™ code generated to calculate $f_{c,insert}$ and the overall shielding effectiveness vs. frequency of the waveguide based on equation (3).

III. PHYSICAL WAVEGUIDE SAMPLES

Four samples consisting of commercially-available waveguides were procured. Relevant parameters for these samples are listed in Table 1. The first waveguide (Sample 1) contained no inserts and was utilized as a reference. The remaining three samples (Samples 2-4) each contained a honeycomb insert, with the dimensions of an individual insert varying from waveguide to waveguide.

All waveguide samples consisted of a main body with a nominal length of 101.6 mm, and a nominal inner diameter of 25.4 mm. Of the three waveguides containing a honeycomb insert, the dimension b of an individual insert (as shown in Fig. 1) varied; however, the length L_{insert} was fixed at 25.4 mm and centered within the respective waveguide.

Table 1: Calculated cutoff frequencies for air-filled circular and hexagonal inserts

Sample No.	Insert Opening $2b$ (mm)	b (mm)	a_L (mm)	$f_{c,insert}$ Eqn. (1) (GHz)	$f_{c,insert}$ Eqn. (5) (GHz)
1*	N/A	N/A	12.75*	6.922*	N/A*
2	6.350	3.175	2.75	31.972	29.830
3	4.764	2.382	2.06	42.629	39.773
4	3.176	1.588	1.37	63.944	59.660

*Sample No. 1 is an open, circular WG with an inner diameter of 25.4 mm.

The radius a of an open, circular waveguide insert was used to calculate the corresponding cutoff frequency f_c. The radius a_L (Fig. 1) of the inscribed circle in a honeycomb insert:

$$a_L = \frac{\sqrt{3}}{2}b, \tag{6}$$

was used to calculate $f_{c,insert}$ of a single honeycomb insert. Cutoff frequencies of a single, air-filled, honeycomb insert using equations (1) and (5) for each sample are shown in Table 1. Samples 1 and 2 were selected for both modeling in FEKO and shielding effectiveness measurements. Samples 3 and 4 were not tested, as the upper end of the frequency range of the available test equipment was limited to 40 GHz.

IV. CREATION OF WAVEGUIDE MODELS

A. Construction of the model

A model was constructed for each sample using Altair Hyperworks® CADFEKO in order to analyze the shielding effectiveness of each configuration. Variables were assigned in the model to represent the dimensions of the waveguide and insert [10]. Construction of the overall waveguide was a straightforward task; however, three steps were necessary to create the honeycomb insert.

The first step in creating the model was to construct a single hexagonal waveguide insert with insert length L_{insert} and the length of a single side b. Both values were set to be equivalent to those of the physical sample as provided by the waveguide manufacturer, with a maximum dimension of $2b$ for the cross-section of a single hexagonal waveguide. This is shown in Fig. 2.
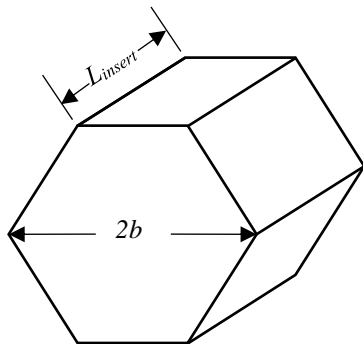
Fig. 2. Dimensions of a single hexagonal insert within the overall honeycomb insert.

The second step in creating the model was to duplicate the single hexagonal waveguide in order to construct the overall honeycomb insert waveguide (HCWG) model. By duplicating and using the *union* function in CADFEKO, the larger insert structure was constructed. This is shown in

Fig. 3 for an insert having thirty-seven (37) individual cells.

By using the variables L_{insert} and b when constructing a single insert as indicated in the previous paragraph, the overall size of the insert structure is automatically adjusted in CADFEKO.

The final step was to combing the HCWG insert model with the larger surrounding waveguide to form the overall model. Adjustment of the relevant dimensions of both the HCWG insert and the surrounding waveguide cylinder required cells of the HC insert falling outside the walls of the surrounding WG cylinder to be trimmed, with partial cells remaining within the interior of the larger WG. Using the dimensions supplied in Table 1, a model was constructed for Sample Number 2 as shown in Fig. 4.
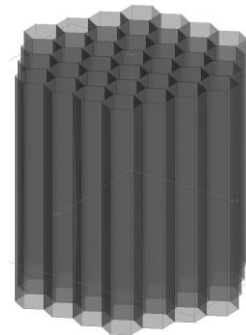
Fig. 3. Hexagonal insert with 37 cells.

The walls of both the main waveguide and the HC inserts were defined in CADFEKO as being constructed of perfect electric conductors (PEC). The medium within the waveguide was initially chosen to be air (ε_r, $\mu_r \approx 1$). By selecting different values for the dielectric constant or relative permittivity of the medium in the waveguide, the model may also be used to simulate a waveguide filled with liquid coolants, e.g., distilled water, ethylene glycol, etc.

B. Preparation for simulation

In the FEKO model, both ends of the waveguide were closed off and designated as waveguide ports. The port located at the $-z$ end of the waveguide was designated as the excitation port (Port 1), and the port at the $+z$ end of the waveguide as the load (Port 2). This is shown in the overall CADFEKO model used to simulate the waveguide with a honeycomb insert in Fig. 4.

Several advantages are realized by utilizing waveguide ports in FEKO. First, FEKO treats these ports by FEKO as being impedance-matched to the waveguide [11]. Second, the need to construct models for transmitting and receiving broadband antennas at either end of the waveguide is eliminated, along with the need to model

an intervening ground plane in which to mount the waveguide. Finally, this reduces the computational resources needed to perform the simulation by reducing the number of elements in the model. A simple solution request for S_{21} is all that is required for FEKO to calculate the shielding effectiveness of the waveguide model.
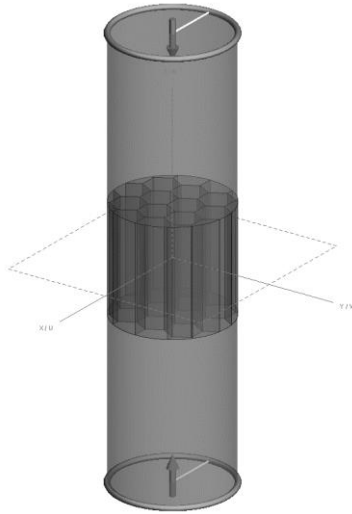
Fig. 4. Combined CADFEKO model for Sample Number 2 with $2b$ = 6.350 mm and L_{insert} = 25.4 mm.

Once the ports were defined, a mesh of the model was created in CADFEKO. This mesh subdivided the model into individual elements in order to use the Finite Element Method (FEM). A coarse mesh size was initially selected to reduce simulation time, resulting in the length of one side of an individual element to be one-sixth the wavelength at the highest simulation frequency, or λ/6 [11]. The selection of this coarse mesh size, however, comes at a cost of reduced accuracy in the calculations for the selected waveguide propagation mode.

Table 2: Mesh size and average edge length

Simulation Frequency Range (GHz)	Mesh Size	Number of Elements	Average Edge Length (mm)
1-18	Coarse	6420	2.276
18-21.5	Standard	32245	0.9811
21.5-28	Standard	43768	0.8424
28-34	Standard	65350	0.6889

A coarse mesh was sufficient for the open WG model (Sample No. 1), but feedback received from the FEKO solver during simulation of the HCWG model (Sample No. 2) resulted in the selection of the standard size mesh. The mesh size (e.g., length of an individual element's edge) also varied based on the maximum frequency for each simulation run. This is shown in Table 2 for both the open waveguide and HCWG models.

C. Simulation methods and calculations

The finite element method (FEM) was chosen to perform the simulation, with the Method of Moments (MoM) solution decoupled from the FEM solution in FEKO. This method is appropriate for complex structures when far-field simulation results (e.g., modeling of antenna patterns) are not required [11].

In the simulation, the ports of the cylindrical waveguide are the circular cross-sections at each end of the cylindrical waveguide. By designating one end of the cylindrical waveguide as the input or active port, FEKO treats the associated cross-section as the plane of excitation. The other end of the waveguide is then treated as an inactive or passive port [12].

The treatment of the ends of the waveguide as matched ports permitted the use of S-parameters to quantify the attenuation, or shielding effectiveness of the waveguide model. S_{21} is defined as the forward transmission coefficient through a network, i.e., the power exiting port 2 with respect to the power incident on port 1 [13]:

$$S_{21} = \frac{b_2}{a_1}\bigg|_{a_2=0}. \tag{7}$$

Calculation of the S-parameters in FEKO for the various waveguide models corresponded well with the planned use of a network analyzer for laboratory measurements, as the network analyzer may be configured to present the results in this format.

The configuration-specific request in FEKO to perform this S-parameter analysis used the dominant TE_{11} mode for both the input and output ports. The input port was selected to be the active port, with application of the dominant TE_{11} mode as the source excitation.

To simplify comparison of the results from the simulation with the analytical and measured shielding effectiveness of the waveguide, a common set of frequencies was chosen. These are shown in Table 3.

Table 3: Frequency information analysis, simulation, and measurement

Frequency Range (GHz)	Number of Points	Frequency Step Size (MHz)
1 to 5	17	250
5 to 7	81	25
7 to 18	45	250
18 to 28	41	250
28 to 34	61	100

V. WAVEGUIDE SHIELDING EFFECTIVENESS MEASUREMENTS

Following the methodology of McInerney [1], a test setup was created to measure the shielding effectiveness of the HCWG. The setup utilized a shielded enclosure, a network analyzer, two (2) sets of matched broadband antennas, and coaxial cables appropriate for the frequency range of interest.

Measurements were performed in four (4) configurations:

a) Antenna to antenna coupling at 2 m distance.
b) Coupling through 25.4 mm (1 in.) circular aperture, 1 m distance to aperture.
c) Coupling through 25.4 mm (1 in.) inner diameter open WG, 1 m distance to waveguide opening.
d) Coupling through 25.4 mm I.D. waveguide with $N = 14$ openings HCWG insert, $b = 3.175$ mm, 1 m distance to waveguide opening.

A general illustration of each of these configurations is shown in Fig. 5. In each case the boresight of the transmitting antenna was visually aligned with that of the receiving antenna, aperture, and/or waveguide opening.

Each configuration was chosen to serve a specific purpose. Configuration a) was utilized to determine the free-space loss between the transmitting and receiving antennas. Configuration b) was used to characterize the coupling loss associated with the transfer of energy from the incident wave to the waveguide as a first-order approximation.
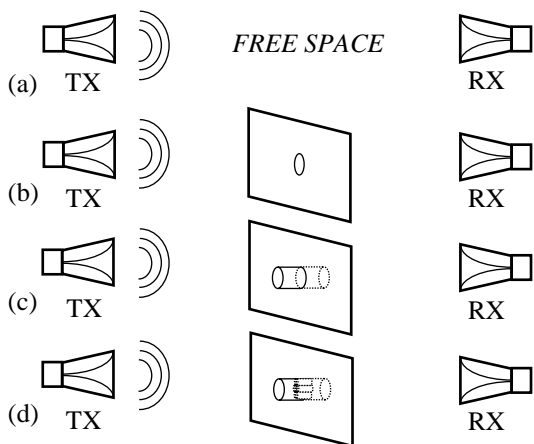
Fig. 5. Test setups for measuring shielding effectiveness of the various configurations.

Configurations c) and d) measured the shielding loss of the entire signal chain, i.e., antenna to waveguide to antenna. The transmit antenna was located external to the shielded enclosure for configurations b)-d); this was intended to prevent reception of unintended signals from the external electromagnetic environment at frequencies below f_c. Cable loss and the preamplifier used for 18 GHz

to 34 GHz was characterized over each frequency range of interest. The network analyzer was verified to be within calibration, and configured to perform a sweep using the frequencies indicated in Table 3. A measurement bandwidth of 1 Hz was used when measuring S_{21} to ensure the highest possible dynamic range in accordance with the manufacturer's datasheet for the network analyzer [14].

A. Definition of various factors which contribute to the overall measurement

The measurement of S_{21} with the waveguide installed may be represented by the following equation:

$$S_{21} = G_T + PL + CP_{WG} + SE_{WG}$$
$$+D_{WG} + PA + G_R + CL. \tag{8}$$

The individual factors are:

- G_T Gain of the transmitting antenna,
- PA Preamplifier gain,
- PL Free space path loss using Friis equation.
- CP_{WG} Losses associated with the coupling of the incident electromagnetic field to the waveguide opening,
- SE_{WG} Shielding effectiveness of the waveguide,
- D_{WG} Directivity of the waveguide opening,
- G_R Gain of the receiving antenna,
- CL Cable losses associated with the test setup.

Prior to starting the measurement series, values for the cable losses CL and preamplifier gain PA are measured using the same network analyzer, and saved for future use in subsequent calculations.

B. Use of the various configurations to determine the contribution(s) of each individual factor

Configuration a) was used to measure the free space path loss PL between the antennas; this is shown in Fig. 5 (a). This measurement was performed in a semi-anechoic chamber of dimensions 4.88 m x 6.10 m x 3.05 m. Photos of the setup are shown in Fig. 6 for the frequency range of 1 GHz to 18 GHz, and Fig. 7 for the frequency range of 18 GHz to 40 GHz.

The distance between the antennas was 2 m. This corresponds to twice the distance between the antenna and the opening of the waveguide.
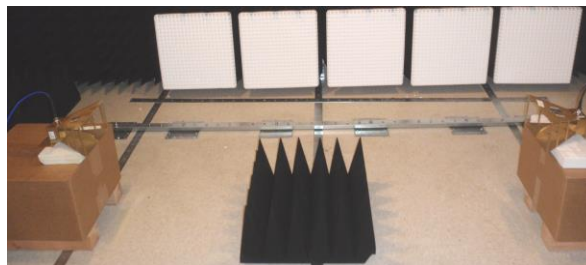
Fig. 6. Test setup for measuring free space loss 1 GHz to 18 GHz (A.H. Systems, Inc. SAS-571 antennas).
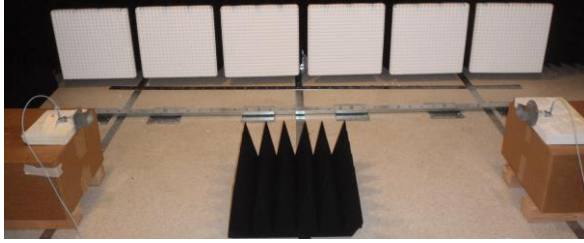
Fig. 7. Test setup for measuring free space loss 18 GHz to 40 GHz (AH-840 Com-Power antennas).

The square patch of absorber located at the center was determined through experimentation to reduce reflections from the ground plane and reduce the variability of the measurement. Measured values for *PL* are calculated using equation (8), with CP_{WG}, SE_{WG}, and G_{WG} set equal to zero, and applying the antenna gains G_T and G_R from calibration.

The measured values for path loss were compared with the theoretical value using the Friis transmission equation with $D = 2$ m:

$$PL = 20\log_{10}\left(\frac{\lambda}{4\pi D}\right). \qquad (9)$$

Configuration b) was used to measure the combined contribution of CP_{WG} and D_{WG} to the measurement. This measurement was performed using the same semi-anechoic chamber; however, the transmit antenna was placed outside the chamber, and the receive antenna was located inside the chamber. The aperture was cut into a bulkhead panel, with the aperture having the same diameter as the inner diameter of the waveguide. The transmit antenna was placed outside the chamber at a distance of 1 m (39.37 in.) from the panel, with the boresight focused on the opening. The receive antenna was placed inside the chamber at the same distance from the panel, with the boresight similarly focused on the opening in the panel. The setup of the transmit antenna external to the semi-anechoic chamber is shown in Fig. 8.

Fig. 8. Transmit antenna position (external to the chamber) for measuring coupling of the electromagnetic wave through the opening, 18 GHz to 40 GHz.

This measurement arrangement provided a combined value for the loss associated with the coupling of the incident electromagnetic wave to the aperture CP_{WG}, and the directivity associated with the wave passing through the aperture D_{WG} while minimizing the attenuation of the wave as it passes through the aperture.

Configuration c) utilized waveguide Sample No. 1 described in Table 1. This waveguide was mounted in the panel opening as shown in Fig. 9.
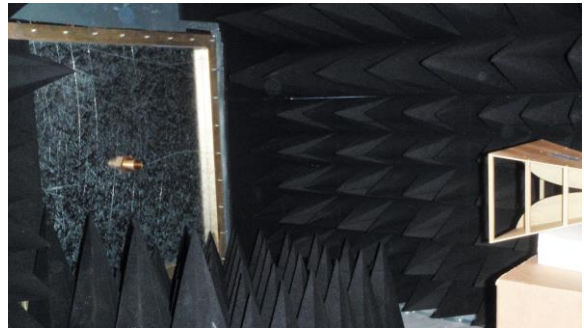
Fig. 9. Receive antenna position (inside the chamber) for measuring coupling of the electromagnetic wave through the opening, 1 GHz to 18 GHz.

Configuration d) used the same setup as shown in Fig. 9, except the open waveguide was replaced with a waveguide sample containing a honeycomb insert.

VI. COMPARISON OF ANALYTIC, SIMULATION, AND MEASURED HCWG SHIELDING EFFECTIVENESS

Shielding effectiveness (SE) measurements were performed on an open waveguide and on a waveguide consisting of $N = 14$ HCWG inserts with a dimension $2b = 6.35$ mm as shown in Fig. 2. These are listed as Sample No. 1 and Sample No. 2 in Table 1, respectively.

The frequency range of the measurements was selected based on the cutoff frequency of the respective waveguide sample. The shielding effectiveness of Sample No. 1 was measured over the frequency range of 1 GHz to 18 GHz, and the shielding effectiveness of Sample No. 2 was measured over the frequency range of 18 GHz to 34 GHz. Both samples were air-filled, i.e., ε_r, $\mu_r \approx 1$.

In comparing the results obtained by measurement and simulation, it should be noted the prediction *a priori* of a theoretical level of agreement between simulation and measurement requires determination of the coupling mechanism between the incident TEM wave and the opening of the waveguide, with the required analyses beyond the scope of this paper. The application of the measurement method presented in Section V is intended to facilitate the calculation of the shielding effectiveness of the waveguide from the measurement results, through

the empirical determination of the coupling loss associated with the transfer of energy from the incident electromagnetic wave to the entrance of the waveguide, and the diffraction of the wave exiting the waveguide at the opposite end.

A. Comparison of analytic and simulation results with SE measurements for the open waveguide model

The shielding effectiveness of the open waveguide was measured over the frequency range of 1-18 GHz using the configuration of Fig. 5 (c). Equation (2) was used to predict the shielding effectiveness of the open waveguide, with equation (1) used to calculate the cutoff frequency f_c. A comparison of the measured results to the predicted values of the open waveguide and values obtained by simulation using FEKO indicated a difference in shielding effectiveness below the predicted cutoff frequency. This is shown in Fig. 10.
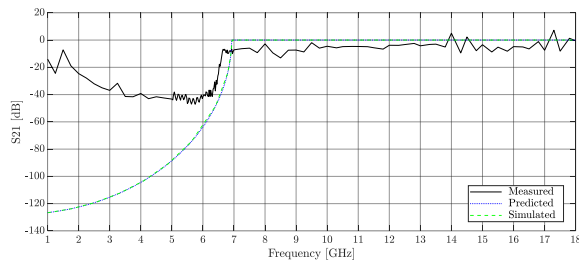
Fig. 10. Comparison of measurement results with predicted and simulated shielding effectiveness values for an open waveguide model with radius $a = 12.7$ mm, 1 GHz to 18 GHz.

The difference in shielding effectiveness below the cutoff frequency of the waveguide was determined to be the result of two factors when extracting the contribution of the open waveguide's shielding effectiveness from the overall measurement. The primary factor is the values of S_{21} for frequencies lower than 6.28 GHz are below the threshold value of -115 dBm necessary for the network analyzer to accurately measure the magnitude of S_{21}. This threshold value was calculated from the applied source power of +10 dBm and the typical dynamic range of 125 dB as specified by the manufacturer [14]. The secondary factor is the measurement uncertainty of S_{21} increases as the magnitude of S_{21} decreases. The values for S_{21} between 6.28 GHz and 6.6 GHz are lower than -90 dB, the value at which the manufacturer no longer provides typical values for the measurement uncertainty. Above 6.6 GHz the measured values for S_{21} were in the range of -80 dB to -90 dB and considered to be reliable.

The shift in cutoff frequency between the predicted and measured shielding effectiveness values was determined to be related to the radius of the sample open waveguide. Measurements of the diameter of the open waveguide showed the radius to be $a = 13.49$ mm (1-1/16 in.), resulting in a revised calculated value of $f_c = 6.517$ GHz for the open waveguide.

B. Comparison of analytic and simulation results with SE measurements for the $b = 3.175$ mm HCWG model

Calculation of $f_{c,insert}$ for a single $b = 3.175$ mm HCWG insert using equations (1) and (5) initially relied on the nominal dimensions ($2b = 0.25$ inch) provided in the waveguide manufacturer's literature. These values are listed in Table 1. Equation (3) was then used to predict the shielding effectiveness over the frequency range of 18-34 GHz of a waveguide having a HCWG insert structure compromised of $N = 14$ individual honeycomb inserts.

Measurement of Sample No. 2 using the configuration of Fig. 5 (d), however, revealed the cutoff frequency of the sample was significantly lower than the predicted value using equation (3) for both the circular and hexagonal calculations. A comparison of the measured results and predicted shielding effectiveness values is shown in Fig. 11.
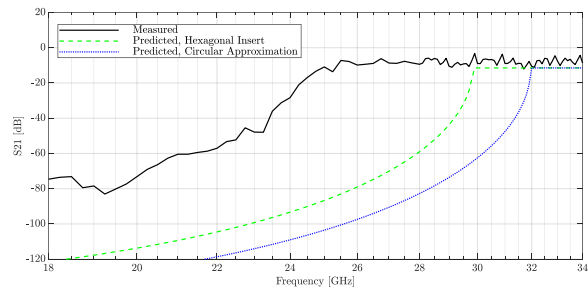
Fig. 11. Comparison of measurement results with predicted shielding effectiveness values for $b = 3.175$ mm, 18 GHz to 34 GHz.

After thoroughly checking the test setup for errors, closer inspection of the HCWG revealed the hexagonal inserts did not exactly match the manufacturer's specified dimension. The cross-sectional area was also observed to be asymmetric, i.e., measurement of a sample of three (3) individual hexagonal cross-sections produced different results for each cross-section. The circular approximation was discarded, and equation (5) applied for calculation of the predicted values of $f_{c,insert}$.

The cutoff frequency of a single insert in the sample was estimated from the data to be approximately 25 GHz. Using equation (5) with a value of $f_{c,insert} = 25$ GHz, a predicted value of $b=3.788$ mm was obtained. The average value for measurements of three (3) individual HC inserts in Sample No. 2 was $b=3.737$ mm. The corresponding cutoff frequency for an individual insert in Sample No. 2 was then calculated using equation (5) to be $f_{c,insert} = 25.347$ GHz. Figure 12 shows the

comparison of the measured results for Sample No. 2 with the revised values for the predicted shielding effectiveness of the waveguide using equation (3) with $N = 14$, and equation (5) for the cutoff frequency of a single HCWG insert.
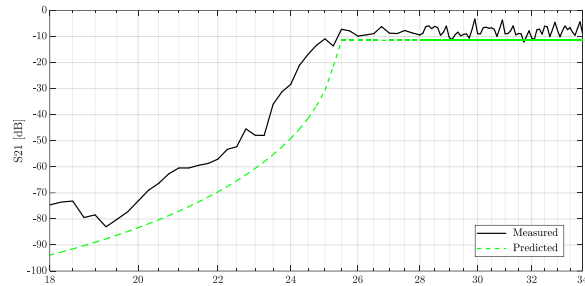
Fig. 12. Comparison of measurement results with the revised predicted shielding values for $b = 3.737$ mm, 18 GHz to 34 GHz.

Based on this new information, the HCWG model with $N = 14$ inserts used in the FEKO simulation was modified to be consistent with the actual, and not the published dimensions of Sample No. 2. The FEKO simulation was repeated, and the results were compared with the predicted and measured shielding effectiveness values over the frequency range 18 GHz to 28 GHz. This comparison is shown in Fig. 13.
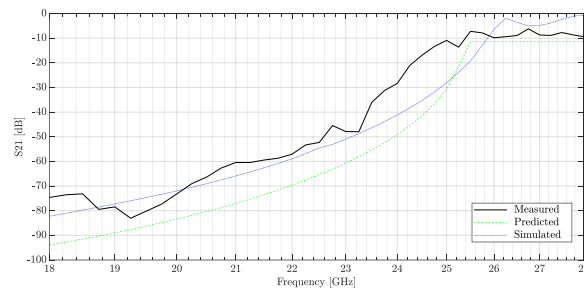
Fig. 13. Comparison of measurement results with predicted and simulated shielding effectiveness values for $b = 3.737$ mm, 18 GHz to 28 GHz.

C. Discussion of results

The predicted shielding effectiveness of an open waveguide based on equation (2) was consistent with the values obtained through both simulation and measurement when the cumulative effect of losses associated with the measurement setup were considered. Analysis of the measurement data below 6 GHz indicated the values of the cable loss, free-space loss, and coupling losses between the incident wave and waveguide opening, when combined with the predicted shielding effectiveness of the waveguide, were below the nominal dynamic range of the network analyzer, in this case 125 dB [14].

The predicted shielding effectiveness of the waveguide containing a HCWG insert based on equation (3) was within the uncertainty of the measurement above the cutoff frequency of a single HCWG insert. The average value of the measured shielding effectiveness above $f_{c,insert} = 25.347$ GHz was $\bar{x} = -8.16$ dB with the sample standard deviation of $\sigma_{\bar{x}} = \pm1.91$ dB. Treating $\sigma_{\bar{x}}$ as a standard uncertainty, application of a coverage factor of $k = 2$ for a 95% confidence level indicated the variability in the results was consistent with the published uncertainty of ±4 dB from 20 GHz to 40 GHz for the selected network analyzer when performing a S_{21} magnitude measurement [14, 15]. Below this cutoff frequency, equation (3) predicted values for shielding effectiveness higher than those obtained by both measurement and simulation.

VII. CONCLUSIONS

Software modeling and laboratory measurements of waveguide samples with HCWG inserts has assisted in improvement of the original model. The first-order approximation of a single HCWG insert as a circle leads to results for the cutoff frequency of a single insert that exceed the values calculated using the analytical formula presented by Ravelo and Mazari (2010). The contribution to the shielding effectiveness of the waveguide, resulting from the division of the larger waveguide into numerous smaller apertures by installation of the HCWG insert, was lower than that predicted by Kaiser (2006); however, the difference between the predicted value and the average measured value was within the stated measurement uncertainty of the selected network analyzer at frequencies above the cutoff frequency of the insert. Planned future work includes investigation of the difference between measurement and simulation results, and application of the model to liquid-filled waveguides.

REFERENCES

[1] M. K. McInerney, S. Ray, R. McCormack, S. Castillo, and R. Mittra, "The effect of fluids on waveguides below cutoff penetrations as related to electromagnetic shielding effectiveness," Champaign, 1984.

[2] F. Choubani, J. David, and N. E. Mastorakis, "Experiment on the shielding by hollow conducting tubes," *IEEE Transactions on Electromagnetic Compatibility*, vol. 48, no. 2, pp. 342-347, May 2006.

[3] G. G. Medveczky and T. Dickten, "High quality shielding with predictable and verifiable effectiveness," *IEEE*, pp. 565-570, 1999.

[4] L. H. Hemming, "Applying the waveguide below cut-off principle to shielded enclosure design," in *IEEE International Symposium on Electro-magnetic Compatibility*, Anaheim, 1992.

[5] S. W. Faust, "An improved waveguide model to support analysis of electromagnetic shielding for liquid cooled power electronics," in *Proceedings of the 2016 Ground Vehicle Systems Engineering and Technology Symposium (GVSETS)*, Novi, 2016.

[6] C. A. Balanis, Advanced Engineering Electromagnetics. Hoboken, NJ: John Wiley & Sons, 2012.

[7] K. L. Kaiser, Electromagnetic Shielding. Boca Raton: CRC Press, 2006.

[8] C. R. Paul, Introduction to Electromagnetic Compatibility. K. Chang, Ed., New York: John Wiley & Sons, 1992.

[9] B. M. B. Ravelo, "Characterization of the regular polygonal waveguide for the RF EM shielding application," *Progress in Electromagnetics Research*, vol. 12, no. M, pp. 95-105, 2010.

[10] Altair Engineering, Inc., *Hyperworks 14.0 Release FEKO*, Troy, Michigan: Altair Engineering, Inc., 2016.

[11] Altair, FEKO Training Class (Suite 7.0) Course Notes, Troy, Michigan: Altair, 2015.

[12] Altair, User Manual for FEKO 14.0, Troy, Michigan: Altair, 2015.

[13] Agilent Technologies, *Agilent AN 154 S-Parameter Design Application Note*, United States: Agilent Technologies, 2000.

[14] Rohde & Schwarz, "www.rohde-schwarz.com," 22 March 2017. [Online]. Available: https://cdn.rohde-schwarz.com/pws/dl_downloads/dl_common_library/dl_brochures_and_datasheets/pdf_1/service_support_30/ZNB_dat-sw_en_5214-5384-22_v0900_96dp.pdf. [Accessed 8 December 2017].

[15] United Kingdom Accreditation Service, *The Expression of Uncertainty in EMC Testing*. 1 ed., Feltham, Middlesex: UKAS, 2002.

Scott W. Faust is an Electrical Engineer with the Vehicle Electronics and Architecture (VEA) group at the U.S. Army Tank Automotive Research, Development and Engineering Center (TARDEC) in Warren, Michigan, USA. He received the B.S. degree in Electrical Engineering from the Rose- Institute of Technology, USA, in 1990, and the M.S. degree Hulman in Electrical and Computer Engineering from Oakland University, USA, in 1994. Mr. Faust is presently a Ph.D. Candidate in the School of Engineering and Computer Science (SECS) at Oakland University. In addition, Mr. Faust is a Part-Time Faculty/ Lecturer at Oakland University, where he teaches a graduate course in electromagnetic engineering. Mr. Faust is certified by the International Association for Radio, Telecommunications, and Electromagnetics (iNARTE) as an Electromagnetic Compatibility Engineer.

Daniel N. Aloi is a Professor and Department Chair in the Electrical and Computer Engineering Department, and the Founding Director of the Applied Electromagnetics and Wireless Lab at Oakland University in Rochester, Michigan, USA. He received his B.S., M.S. and Ph.D. degrees in Electrical Engineering from Ohio University in 1992, 1996 and 1999, respectively. He has been employed at Oakland University since January 2002. Aloi was a Sr. Project Engineer at OnStar, Inc. (2000-2001) and a Visiting Assistant Professor at Ohio University (1999-2000). His research areas include applied electromagnetics and various areas of the global positioning system (GPS) in the automotive and aviation industries. He has authored over 90 papers and six patents.